

Local elastic fields around cracks and their stress density of states

Stefano Giordano* and Luciano Colombo†

Department of Physics of the University of Cagliari and Sardinian Laboratory for Computational Materials Science (SLACS, INFN-CNR), Cittadella Universitaria, I-09042 Monserrato (Ca), Italy

(Received 16 July 2007; revised manuscript received 26 September 2007; published 30 November 2007)

The exact local elastic fields around a slit or circular crack under load are calculated by means of a generalized version of the Eshelby theory, where the flat shape of the crack is correctly accounted for. The concept of density of states is then introduced and applied in characterizing the fluctuations of the nearby elastic stress field.

DOI: 10.1103/PhysRevB.76.174120

PACS number(s): 46.50.+a, 62.20.Mk, 62.25.+g

I. INTRODUCTION

The investigation on the mechanical properties of heterogeneous, composite, or imperfect materials has been primarily focused on the search for the effective physical properties exhibited at the macroscopic scale.^{1,2} Typically, such investigation is based on homogenization techniques: at first, the exact mathematical analysis of the mechanical behavior induced by a single defect (like an inclusion, an inhomogeneity, or a crack)³ is worked out; then, the analysis is completed by considering the interactions among the defects,^{4,5} in the limit of low density. Such a hypothesis can be partially removed by means of the iterated homogenization⁶ or by differential schemes.^{7,8} These techniques have been applied both to the case of embedded inhomogeneities^{9,10} and to the case of dispersed defects, such as microcracks in a matrix.^{11–13} A common feature of all effective medium theories is that the actual microscopic details of the investigated physical quantities are coarse grained. For example, strain and stress fields are averaged over a suitable region and the possible local fluctuations are, therefore, neglected.

It has been widely recognized that different methodologies must be concurrently integrated in order to properly model the interplay between phenomena occurring at different length scales. This idea leads to the multiscale approach: a paradigm effectively coupling different methods and thus providing a unique theoretical device able to pass physical information across different scales.¹⁴ For example, the above macroscopic continuum homogenization theories can be linked to atomistic simulations, which describe the complex behavior of a given system at the nanoscale, i.e., at the most fundamental level.¹⁵ Sometimes, different techniques may lead to the same result at a given length scale. An important and relevant example is given by the atomistic validation¹⁶ of the continuum stability theory¹⁷ for crack propagation in ideally brittle, single-crystal materials.

Despite several efforts toward the multiscale paradigm, little attention has been so far devoted to the quantitative evaluation of the local fluctuations of elastic fields in the neighborhood of an inhomogeneity (e.g., a crack, an inclusion, or a void). Such fluctuations can easily extend over a spatial domain so large to result out of reach for atomistic simulations. On the other hand, homogenization theories simply do not take these features into account. This situation is similarly found when studying the physics of nonhomogeneous dielectric continua.^{18–21}

In this work, we address the determination of the elastic fields (namely, displacement, strain, and stress) around a crack, when the elastic region is under uniform external loading. We work out our theory in the framework of continuum mechanics (linear elasticity) and we introduce the concept of density of states (DOS) for the stress field. The main goal is twofold: (i) characterizing (analytically) the spatial distribution of the elastic fields nearby the crack and (ii) evaluating (numerically) their local fluctuations by means of the stress DOS.

As for the first goal, we consider two paradigmatic geometrical configurations (i.e., slit and circular) of a single crack under load. They are represented in Figs. 1 and 2, respectively.

These canonical problems contain all the features of interest in linear elastic fracture mechanics (LEFM).²² The key idea is to calculate the displacement field by means of a novel methodology based on the Eshelby theory.^{23,24} In its original formulation, such a formal set copes with the problem of finding the elastic perturbation induced by the presence of an ellipsoidal inclusion embedded into a linear, isotropic, and homogeneous medium under uniform loading. The slit or circular shape of a given crack can be obtained by a suitable transformation of an ellipsoidal void and, therefore, they both correspond to a limiting case of the standard Eshelby theory.

A huge body of knowledge has been developed in the framework of LEFM about the above topics. For instance,

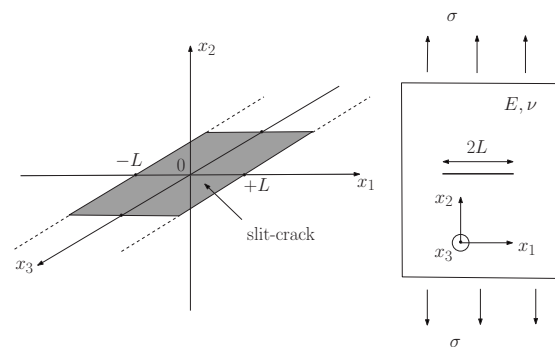


FIG. 1. Left panel: geometry of a slit crack lying in the (x_1, x_3) plane. Right panel: elastic medium (with the Young modulus E and the Poisson ratio ν) containing a slit crack (with length $2L$) under uniaxial stress σ (along x_2).

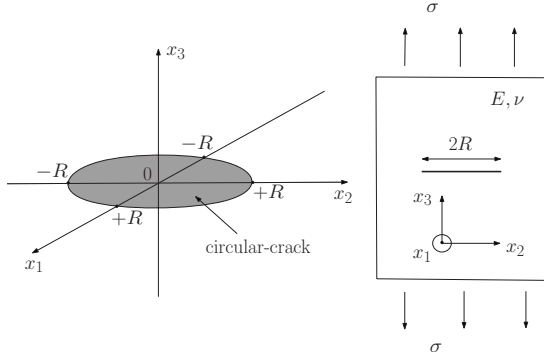


FIG. 2. Left panel: geometry of a circular crack lying in the (x_1, x_2) plane. Right panel: elastic medium (with the Young modulus E and the Poisson ratio ν) containing a circular crack (with radius R) under uniaxial stress σ (along x_3).

the singular behavior of the stress near the end of a slit crack or near sharp corners has been found in several pioneering works.^{25–29} Moreover, circular cracks have been studied by using integral equations and integral transforms.^{30–32} Nevertheless, we remark that the existing results always represent an *ad hoc* solution for a given particular case. Under this respect, the first goal of the present study is aimed at reconciling different LEFM results into a self-contained general theory.

The second issue of the present work consists in the use of the DOS as a tool to characterize some relevant mechanical quantities, notably the stress field. If we subdivide a region containing a crack under loading in a large number of very small domains and we count the number of domains in which a given component T_{ij} of the stress tensor has values in the interval $(\tau, \tau + \Delta\tau)$, then we can effectively define the stress density. Such a definition is fully developed in Sec. V, where we also show that the stress DOS displays singularities. We prove that this theoretical concept is a valuable tool to quantify the space distribution of any tensor field (or its components).

The structure of the present paper is the following. In Sec. II, we present an outline of the Eshelby theory. In Secs. III and IV, we develop the theory for the slit crack and for the circular crack, respectively. Finally, in Sec. V, we introduce the concept of DOS for the stress and we discuss some notable applications.

II. OUTLINE OF THE ESHELBY THEORY

Let an ellipsoidal inclusion Ω be embedded into a matrix, remotely loaded by uniform external forces (see Fig. 3, right).

The homogeneous solid matrix (hereafter referred to as material 1) is characterized by the relation $\hat{T} = \hat{C}^{(1)} \hat{\epsilon}$ or, equivalently, $T_{ij} = C_{ijkh}^{(1)} \epsilon_{kh}$, where \hat{T} is the stress tensor (with components T_{ij}), $\hat{\epsilon}$ is the strain tensor (with components ϵ_{ij}), and $\hat{C}^{(1)}$ is the stiffness tensor represented by the elastic constants $C_{ijkh}^{(1)}$. In a similar way, the elastic properties of the embedded (uniform) inclusion are described by the tensor

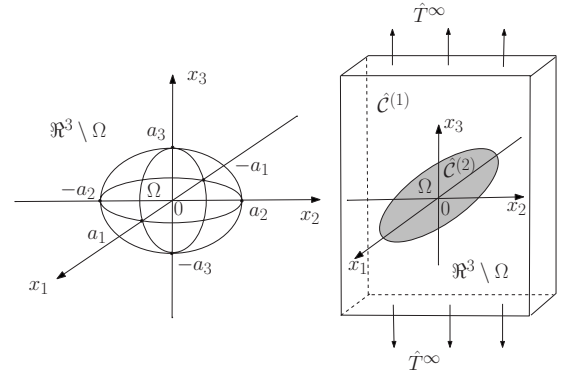


FIG. 3. Left panel: geometry of an ellipsoidal inclusion. Right panel: elastic medium (with stiffness tensor $\hat{C}^{(1)}$) occupying the volume $\mathfrak{R}^3 \setminus \Omega$ and including an inhomogeneity (with stiffness tensor $\hat{C}^{(2)}$) of volume Ω under arbitrary loading \hat{T}^∞ .

$\hat{C}^{(2)}$ having elements $C_{ijkh}^{(2)}$. We choose a reference frame defined by three fixed Cartesian orthogonal axes, as shown in Fig. 3, where the position vector is $\vec{r} = (x_1, x_2, x_3)$. In the present work, we adopt the Voigt notation; therefore, the six-element strain and stress vectors are written as

$$\tilde{\epsilon} = [\epsilon_{11} \quad \epsilon_{22} \quad \epsilon_{33} \quad \epsilon_{12} \quad \epsilon_{23} \quad \epsilon_{13}]^T,$$

$$\tilde{T} = [T_{11} \quad T_{22} \quad T_{33} \quad T_{12} \quad T_{23} \quad T_{13}]^T, \quad (1)$$

where $[\cdot]^T$ means the transposed vector. By adopting this notation scheme, the stiffness four-index tensor for both the isotropic solid and the inclusion is represented by a 6×6 matrix

$$\tilde{C}^{(n)} = \begin{bmatrix} \mathfrak{a}^{(n)} & \mathfrak{b}^{(n)} & \mathfrak{b}^{(n)} & 0 & 0 & 0 \\ \mathfrak{b}^{(n)} & \mathfrak{a}^{(n)} & \mathfrak{b}^{(n)} & 0 & 0 & 0 \\ \mathfrak{b}^{(n)} & \mathfrak{b}^{(n)} & \mathfrak{a}^{(n)} & 0 & 0 & 0 \\ 0 & 0 & 0 & 2\mu^{(n)} & 0 & 0 \\ 0 & 0 & 0 & 0 & 2\mu^{(n)} & 0 \\ 0 & 0 & 0 & 0 & 0 & 2\mu^{(n)} \end{bmatrix}, \quad (2)$$

where $\mathfrak{a}^{(n)} = k^{(n)} + \frac{4}{3}\mu^{(n)}$ and $\mathfrak{b}^{(n)} = k^{(n)} - \frac{2}{3}\mu^{(n)}$ are simple combinations of the elastic moduli. The index $n=1, 2$ refers to the matrix and inclusion, respectively, while the elastic moduli are named k (bulk modulus) and μ (shear modulus). The stress-strain relation is accordingly cast in the form $\tilde{T} = \tilde{C}^{(1)} \tilde{\epsilon}$ within the matrix (i.e., in $\mathfrak{R}^3 \setminus \Omega$) and $\tilde{T} = \tilde{C}^{(2)} \tilde{\epsilon}$ inside the embedded particle (i.e., within Ω). The bulk and the shear moduli can be replaced when needed by the Young modulus $E^{(n)} = \frac{9k^{(n)}\mu^{(n)}}{\mu^{(n)} + 3k^{(n)}}$ and the Poisson ratio $\nu^{(n)} = \frac{3k^{(n)} - 2\mu^{(n)}}{2(\mu^{(n)} + 3k^{(n)})}$.

We suppose that the forces remotely applied generate a uniform elastic deformation when no inclusion is present into the body. The corresponding elastic state is fully described by the linear displacement $u_i^\infty(\vec{r})$, by the uniform strain $\epsilon_{kh}^\infty = \frac{1}{2} \left(\frac{\partial u_k^\infty}{\partial x_h} + \frac{\partial u_h^\infty}{\partial x_k} \right)$, and by the uniform stress $T_{ij}^\infty = C_{ijkh}^{(1)} \epsilon_{kh}^\infty$. If we now embed the inclusion into the matrix, we must evaluate the perturbation to such elastic fields both in-

side and outside the inclusion. Firstly, we define the total displacement as the sum of the unperturbed displacement u_i^∞ and a perturbation u_i^p induced by the insertion

$$u_i = u_i^\infty + u_i^p. \quad (3)$$

Following the Eshelby theory, the perturbation u_i^p is the displacement corresponding to the equivalent eigenstrain (mimicking the inclusion) defined by

$$\tilde{\epsilon}^* = \{[\tilde{I} - (\tilde{C}^{(1)})^{-1}\tilde{C}^{(2)}]^{-1} - \tilde{S}\}^{-1}\tilde{\epsilon}^\infty. \quad (4)$$

Details are found elsewhere.³ Here, we have introduced the Eshelby tensor \tilde{S} and the 6×6 identity matrix \tilde{I} . \tilde{S} depends only on geometrical factors of the ellipsoidal inclusion and on the Poisson ratio of the host matrix. In other words, \tilde{S} contains all the physical information needed to predict the mechanical interaction between the inclusion and the matrix under external load.

The displacement u_i^p induced by the equivalent eigenstrain $\tilde{\epsilon}^*$ can be evaluated in terms of the so-called harmonic $\Phi(\vec{r})$ and biharmonic $\Psi(\vec{r})$ potentials^{23,24} as

$$u_i^p(\vec{r}) = \epsilon_{kh}^* \left[\frac{1}{8\pi(1-\nu)} \Psi_{,ikh} - \frac{\delta_{ih}}{4\pi} \Phi_{,k} - \frac{\delta_{ik}}{4\pi} \Phi_{,h} - \frac{\nu}{1-\nu} \frac{\delta_{kh}}{4\pi} \Phi_{,i} \right]. \quad (5)$$

Hereafter, we adopt the symbol $f_{,i} = \frac{\partial f}{\partial x_i}$ and we extend this notation to higher order derivatives. Equations (3) and (5) are valid anywhere. The harmonic potential is defined by the Poisson equation $\nabla^2 \Phi = -4\pi$ if $\vec{r} \in \Omega$, 0 if $\vec{r} \notin \Omega$, and the integral form of its solution is $\Phi(\vec{r}) = \int_{\Omega} \frac{1}{|\vec{r}-\vec{x}|} d\vec{x}$. Similarly, the biharmonic potential is defined by means of the biharmonic equation $\nabla^4 \Psi = -8\pi$ if $\vec{r} \in \Omega$, 0 if $\vec{r} \notin \Omega$, and the standard integral representation^{3,23} is $\Psi(\vec{r}) = \int_{\Omega} |\vec{r}-\vec{x}| d\vec{x}$. Such harmonic and biharmonic potentials only contain geometrical information about the embedded ellipsoid (i.e., the semiaxis lengths).

It is worthwhile recalling some explicit expressions providing the above potentials or their derivative as used to determine the elastic fields³

$$\begin{aligned} \Phi(\vec{r}) &= \pi a_1 a_2 a_3 \int_{\eta(\vec{r})}^{+\infty} \frac{1 - f(\vec{r}, s)}{R(s)} ds, \\ \Psi_{,i}(\vec{r}) &= \pi a_1 a_2 a_3 x_i \int_{\eta(\vec{r})}^{+\infty} \frac{1 - f(\vec{r}, s)}{R(s)} \frac{s}{a_i^2 + s} ds, \end{aligned} \quad (6)$$

where $f(\vec{r}, s)$, $\eta(\vec{r})$, and $R(s)$ are defined as follows:

$$\begin{aligned} f(\vec{r}, s) &= \frac{x_1^2}{a_1^2 + s} + \frac{x_2^2}{a_2^2 + s} + \frac{x_3^2}{a_3^2 + s}, \\ \eta(\vec{r}): \quad &f[\vec{r}, \eta(\vec{r})] = 1, \\ R(s) &= \sqrt{(a_1^2 + s)(a_2^2 + s)(a_3^2 + s)}. \end{aligned} \quad (7)$$

The quantity $\eta(\vec{r})$ is defined in implicit form and it is considered as the largest positive root of the equation

$f[\vec{r}, \eta(\vec{r})] = 1$. The integrals defined in Eq. (6) are used for the external region assuming $\eta(\vec{r})$ given in Eq. (7) and for the internal region assuming $\eta(\vec{r}) = 0$.

For the sake of completeness, we briefly summarize also the solution of the problem in terms of the strain tensor. The perturbation to the strain is defined by the standard relation $\epsilon_{kh}^p = \frac{1}{2} \left(\frac{\partial u_k^p}{\partial x_h} + \frac{\partial u_h^p}{\partial x_k} \right)$ and it can be evaluated accordingly to the relation $\tilde{\epsilon}^p = \tilde{S} \tilde{\epsilon}^*$. Therefore, the total strain $\tilde{\epsilon} = \tilde{\epsilon}^\infty + \tilde{\epsilon}^p = \tilde{\epsilon}^\infty + \tilde{S} \tilde{\epsilon}^*$ [corresponding to the total displacement given in Eq. (3)] can be found through the following relations (Voigt notation):

$$\tilde{\epsilon} = \{ \tilde{I} - \tilde{S} [\tilde{I} - (\tilde{C}^{(1)})^{-1} \tilde{C}^{(2)}] \}^{-1} \tilde{\epsilon}^\infty \quad \text{if } \vec{r} \in \Omega,$$

$$\tilde{\epsilon} = (\tilde{I} + \tilde{S}^\infty \{ [\tilde{I} - (\tilde{C}^{(1)})^{-1} \tilde{C}^{(2)}]^{-1} - \tilde{S} \}^{-1}) \tilde{\epsilon}^\infty \quad \text{if } \vec{r} \notin \Omega, \quad (8)$$

where $\tilde{S}^\infty(\vec{r})$ is the so-called *external* point Eshelby tensor. Finally, the generic form of the Eshelby tensor, which is correct both inside and outside the inclusion, can be written by means of the elastic potentials as follows:²⁴

$$\begin{aligned} \mathcal{S}_{ijkh}(\vec{r}) &= \frac{1}{8\pi(1-\nu)} \Psi_{,ijkh} - \frac{\nu}{1-\nu} \frac{\delta_{kh}}{4\pi} \Phi_{,ij} - \frac{1}{8\pi} (\delta_{ih} \Phi_{,jk} \\ &+ \delta_{ik} \Phi_{,jh} + \delta_{jh} \Phi_{,ik} + \delta_{jk} \Phi_{,ih}). \end{aligned} \quad (9)$$

Usually, the notation adopted for the Eshelby tensor is different for the *internal* points and for *external* ones,

$$\mathcal{S}_{ijkh}(\vec{r}) = \mathcal{S}_{ijkh} \quad \text{if } \vec{r} \in \Omega,$$

$$\mathcal{S}_{ijkh}(\vec{r}) = \mathcal{S}_{ijkh}^\infty(\vec{r}) \quad \text{if } \vec{r} \notin \Omega. \quad (10)$$

Taking a different notation for the internal and the external region is particularly efficient in order to remind that the internal Eshelby tensor is constant and, therefore, the internal stress and strain are uniform tensor fields.

III. SLIT CRACK

The elementary object of our model is an ellipsoidal void with a very small minor axis, so to reproduce the flat shape of a crack. If one of the semiaxes of the ellipsoidal void, say, a_3 , becomes very large and the minor semiaxis a_2 becomes negligibly small, then the ellipsoid reduces to a slitlike crack with semilength $a_1 = L$ (see Fig. 1). In order to correctly perform the limiting process, we start considering a void with infinite a_3 and finite a_2 and a_1 , corresponding to an elliptic cylinder aligned with the x_3 axis. We define the aspect ratio as $e = a_2/a_1 = a_2/L$. The actual slitlike crack geometry will be eventually obtained by the limit $a_2 \rightarrow 0$ or, equivalently, $e \rightarrow 0$. The complete results for the elastic potentials describing this geometry are reported in Appendix A. There, we also verify that the quantities $\Phi_{,i}$ and $\Psi_{,ijk}$ approach zero when the aspect ratio e becomes vanishingly small. This is a point that will play a crucial role in the following development of the theory.

In general, we suppose that the matrix is at first placed in an equilibrium state of uniform elastic strain, due to external

loads. The inclusion is then embedded into the matrix, thus affecting the state of strain, as described by the Eshelby theory. In particular, it is important to notice that the internal strain is uniform provided that the external or bulk strain is uniform. When the physical condition $C_{ijkh}^{(2)}=0$ defining a crack is considered, then the induced internal strain and the equivalent eigenstrain become identical. Their link to the applied external strain,

$$\tilde{\epsilon} = \tilde{\epsilon}^* = [\tilde{I} - \tilde{S}]^{-1} \tilde{\epsilon}^\infty \quad \text{if } \vec{r} \in \Omega, \quad (11)$$

is easily obtained from Eqs. (4) and (8). The eigenstrain $\tilde{\epsilon}^*$ is an important quantity since it appears in Eq. (5) providing the displacement. From now on, the only elastic moduli describing the system are those of the matrix ($\hat{C}^{(2)}=0$ in the crack): therefore, for the sake of simplicity, we proceed by only using the Young modulus E and the Poisson ratio ν of such an isotropic medium. In Eq. (11), the Eshelby tensor \tilde{S} depends on the aspect ratio $e=a_2/a_1$ and on the Poisson ratio ν of the matrix. The exact expression of the Eshelby tensor for the elliptic cylinder is given in Appendix B, where we also prove that the eigenstrain appearing in Eq. (11) is singular when $e \rightarrow 0$.

We now proceed to calculate the exact displacement field around the crack. In the present work, we analyze both the case of pure uniaxial stress and of pure uniaxial strain, both in mode I loading. The components of the total displacement are obtained from Eqs. (3) and (5) in the limit $e \rightarrow 0$,

$$u_i(\vec{r}) = u_i^\infty(\vec{r}) + \lim_{e \rightarrow 0} u_i^p(\vec{r}) = u_i^\infty(\vec{r}) + \lim_{e \rightarrow 0} \frac{\Psi_{,ijk} \epsilon_{kh}^*}{8\pi(1-\nu)} - \lim_{e \rightarrow 0} \frac{\epsilon_{ik}^* \Phi_{,k} - \lim_{e \rightarrow 0} \frac{\nu \epsilon_{kk}^* \Phi_{,i}}{4\pi(1-\nu)}, \quad (12)$$

where the potential derivatives $\Phi_{,i}$ and $\Psi_{,ijk}$ are given in Appendix A, while the term $[\tilde{I} - \tilde{S}]^{-1}$ entering in Eq. (11) for the eigenstrain $\tilde{\epsilon}^*$ is derived in Appendix B. Since in this work we consider the case of pure uniaxial stress as well as of pure uniaxial strain, we must follow different procedures.

A. Pure uniaxial stress conditions

In pure uniaxial stress condition, we apply the load

$$\tilde{T}^\infty = [0 \quad \sigma \quad 0 \quad 0 \quad 0 \quad 0]^T, \quad (13)$$

where the quantity σ represents the tensile stress applied in mode I along the x_2 direction, as represented in Fig. 1, right. The corresponding external strain is simply given by

$$\tilde{\epsilon}^\infty = \begin{bmatrix} -\frac{\nu\sigma}{E} & \frac{\sigma}{E} & -\frac{\nu\sigma}{E} & 0 & 0 & 0 \end{bmatrix}^T. \quad (14)$$

By using Eqs. (11) and (B3), we obtain the equivalent eigenstrain

$$\tilde{\epsilon}^* = \begin{bmatrix} \frac{(2\nu^2-1)\sigma}{E} & \frac{(2-2\nu^2+e)\sigma}{eE} & -\frac{\nu\sigma}{E} & 0 & 0 & 0 \end{bmatrix}^T. \quad (15)$$

The total displacement is eventually calculated through Eq. (12),

$$u_1 = -\frac{\sigma x_1(1+\nu)}{E} \left[\frac{1-2\nu^2}{1+\nu} - \frac{\beta}{\alpha} \sqrt{\frac{\eta}{L^2+\eta}} \right], \quad (16)$$

$$u_2 = \frac{\sigma x_2(1+\nu)}{E} \left[\frac{\nu(1+2\nu)}{1+\nu} + \frac{\beta}{\alpha} \sqrt{\frac{L^2+\eta}{\eta}} \right], \quad (17)$$

$$u_3 = -\frac{\sigma \nu x_3}{E}. \quad (18)$$

We remember that the slit crack is aligned along the x_3 axis and the two surfaces of the crack lie on the plane (x_1, x_3) . The parameters α , β , and η are listed below,

$$\alpha = x_1^2 \eta^2 + x_2^2 (L^2 + \eta)^2,$$

$$\beta = (1-2\nu)(x_1^2 + x_2^2) \eta^2 + 2(1-\nu)x_2^2 L^4 + (3-4\nu)x_2^2 L^2 \eta,$$

$$\eta = \frac{1}{2}(x_1^2 + x_2^2 - L^2) + \frac{1}{2}\sqrt{(x_1^2 + x_2^2 + L^2)^2 - 4L^2 x_1^2}. \quad (19)$$

The expression for η is derived from Eq. (A5) in the limit $e \rightarrow 0$. Equations (16)–(18) (and the similar ones described below for other cases) are important because they describe in a very compact form the displacement field in the whole space. They contain, as particular cases, all the standard LEFM results.

In principle, from Eqs. (16)–(18), it is easy to calculate the strain or the stress tensor in some region of interest, by using the constitutive relation of the matrix. Here, we do not report this calculation since it is rather complicated and does not add any conceptual issue to the present discussion. Rather, we focus on the shape assumed by the crack under loading and we calculate the displacements at the crack surface. In particular, we take into consideration the upper surface of the crack. If $x_2 \rightarrow 0^+$ and $|x_1| < L$, then

$$\eta \rightarrow \frac{L^2}{L^2 - x_1^2} x_2^2 \quad \text{and} \quad \frac{\beta}{\alpha} \rightarrow 2(1-\nu). \quad (20)$$

By using these limiting conditions in Eqs. (16)–(18), we obtain the displacement of the upper crack surface,

$$u_1 = -\frac{\sigma x_1}{E} (1-2\nu^2),$$

$$u_2 = \frac{2\sigma}{E} (1-\nu^2) \sqrt{L^2 - x_1^2}. \quad (21)$$

Incidentally, the same result is found in the Landau and Lifschitz elasticity textbook.³³ There, a different approach to deal with sharp cracks is outlined: the Landau-Lifschitz method exactly provides the results given in Eq. (21) for the

zone of the crack far away from the tips [see Eq. (31.14) of Ref. 33]. On the other hand, the crack tip region is only approximately described, while our present procedure is rigorously valid everywhere.

The typical crack opening displacement (COD) of LEFM is simply given by twice the above quantity u_2 . It is interesting to observe that Eq. (21) confirms that the original crack segment $x_2=0$, $-L < x_1 < L$ in the plane (x_1, x_2) is transformed into an ellipse by the applied forces; in fact, from Eq. (21), one can derive the standard ellipse equation

$$\frac{x_1^2}{\left[1 + \frac{\sigma}{E}(2\nu^2 - 1)\right]^2 L^2} + \frac{x_2^2}{\frac{4\sigma^2(1 - \nu^2)^2 L^2}{E^2}} = 1. \quad (22)$$

Finally, we obtain the T_{22} (opening) component of the stress,

$$T_{22} = \frac{E \left[\nu \left(\frac{\partial u_1}{\partial x_1} + \frac{\partial u_3}{\partial x_3} \right) + (1 - \nu) \frac{\partial u_2}{\partial x_2} \right]}{(1 - 2\nu)(1 + \nu)}, \quad (23)$$

which is reported in Fig. 4. When $x_2=0$, Eq. (23) provides the well known Inglis result,²⁵

$$T_{22} = \frac{|x_1| \sigma}{\sqrt{x_1^2 - L^2}} \quad \text{if } x_2 \rightarrow 0, \quad |x_1| > L. \quad (24)$$

This result is important since it naturally drives to the concept of stress intensity factor (SIF), which was phenomenologically introduced by Irwin.³⁴ Along the x_1 axis, the distance from the tip of the slit crack is given by $x_1 - L$. When a tensile stress σ is applied along the x_2 axis (see Fig. 1), the singular behavior of the stress field near the tip crack is described by the following SIF:

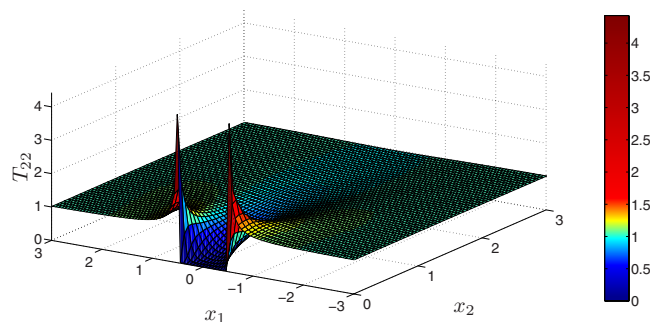


FIG. 4. (Color online) Tensile stress field T_{22} along x_2 in a slit crack. We have assumed the values $E=1$, $\sigma=1$, $\nu=0.33$, and $L=0.5$ in arbitrary units. The region under consideration is described by $-3 < x_1 < 3$ and $0 < x_2 < 3$. The results are represented for pure uniaxial stress conditions. The color map (shown on the right) represents the intensity of T_{22} in arbitrary units.

$$K_I = \lim_{x_1 \rightarrow L, x_2 \rightarrow 0} T_{22} \sqrt{2\pi(x_1 - L)} = \sigma \sqrt{L\pi}. \quad (25)$$

The last equation corresponds to the isotropic version of the remarkable result by Barnett and Asaro.³⁵ The stress intensity factor K_I is independent of elastic moduli. We also remark that the paradigmatic case described in this section was used by Griffith¹⁷ in his theory of crack instability. Stress intensification is confirmed by atomistic simulations as well.¹⁶

B. Pure uniaxial strain conditions

In pure uniaxial strain conditions, the external applied strain is defined as

$$\tilde{\epsilon}^\infty = [0 \quad \delta \quad 0 \quad 0 \quad 0 \quad 0]^T, \quad (26)$$

where δ is the constant strain in the x_2 direction. This strain field is associated with the following applied stress:

$$\tilde{T}^\infty = \begin{bmatrix} \frac{\nu E \delta}{(1 - 2\nu)(1 + \nu)} & \frac{(1 - \nu) E \delta}{(1 - 2\nu)(1 + \nu)} & \frac{\nu E \delta}{(1 - 2\nu)(1 + \nu)} & 0 & 0 & 0 \end{bmatrix}^T. \quad (27)$$

Similarly to the procedure developed in Sec. III A, we define the quantity σ representing the tensile stress applied in mode I (i.e., the element T_{22}^∞) and the quantity δ measuring the strain along x_2 , as respectively, as

$$\sigma = \frac{(1 - \nu) E \delta}{(1 - 2\nu)(1 + \nu)}, \quad \delta = \frac{(1 - 2\nu)(1 + \nu) \sigma}{(1 - \nu) E}. \quad (28)$$

Substituting Eq. (28) into Eq. (26), we obtain the external applied strain in terms of the tensile stress σ ,

$$\tilde{\epsilon}^\infty = \begin{bmatrix} 0 & \frac{(1 - 2\nu)(1 + \nu) \sigma}{(1 - \nu) E} & 0 & 0 & 0 & 0 \end{bmatrix}^T. \quad (29)$$

The components of the total displacement are obtained from Eq. (12),

$$u_1 = -\frac{\sigma x_1 (1 + \nu)}{E} \left[(1 - 2\nu) - \frac{\beta}{\alpha} \sqrt{\frac{\eta}{L^2 + \eta}} \right], \quad (30)$$

$$u_2 = \frac{\sigma x_2 (1 + \nu)}{E} \left[\frac{\nu(1 - 2\nu)}{1 - \nu} + \frac{\beta}{\alpha} \sqrt{\frac{L^2 + \eta}{\eta}} \right], \quad (31)$$

$$u_3 = 0. \quad (32)$$

The parameters α , β , and η are once again given by Eq. (19). Once more, the displacement of the upper crack surface can be obtained by using Eq. (20),

$$u_1 = -\frac{\sigma x_1}{E} (1 - 2\nu)(1 + \nu),$$

$$u_2 = \frac{2\sigma}{E}(1-\nu^2)\sqrt{L^2-x_1^2}. \quad (33)$$

Such relations correspond to an elliptic deformation of the crack surfaces described by

$$\frac{x_1^2}{\left[1 + \frac{\sigma}{E}(2\nu-1)(1+\nu)\right]^2 L^2} + \frac{x_2^2}{\frac{4\sigma^2(1-\nu^2)^2 L^2}{E^2}} = 1. \quad (34)$$

Finally, we remember that the Inglis result given in Eq. (24) and the relative calculation of the SIF given in Eq. (25) are still valid in the same form.

IV. CIRCULAR CRACK

We take now into consideration an ellipsoid of revolution ($a_1=a_2=R$) with the principal axis aligned along x_3 ; we define the aspect ratio e as $e=a_3/a_1=a_3/a_2$, where a_1 , a_2 , and a_3 are the semiaxes aligned, respectively, along the axes x_1 , x_2 , and x_3 of the given reference frame. The geometry of a circular crack is recovered in the limit of $e \rightarrow 0$ (strongly oblate ellipsoid), as one can see in Fig. 2, right. Henceforth, we consider e as a finite quantity and we will perform the limit at the end of the procedure. Furthermore, we calculate

the derivatives of the elastic potentials given in Eqs. (A1) and (A2) under the assumptions $a_1=a_2=R$ and $a_3=eR$. The expressions for such potentials or their derivatives are not reported here for the sake of brevity. By now, the idea should be manifested: we use the displacement as given in Eq. (12) where the eigenstrain is calculated by means of Eq. (11). To evaluate such an eigenstrain, we need the internal Eshelby tensor for ellipsoids of revolution: its structure is described in Appendix C, where the singular behavior of the term $[\tilde{I} - \tilde{S}]^{-1}$ is discussed as well. From this point on, we must impose the external applied forces (or, equivalently, the strain $\tilde{\epsilon}^e$) in order to find out the final results under the pure uniaxial stress and pure uniaxial strain conditions.

A. Pure uniaxial stress conditions

The external forces are characterized by a tensile stress $T_{33}=\sigma$ (see Fig. 2). Such a loading corresponds to the external strain given by Eq. (14), which, by using Eqs. (11) and (C4), provides the asymptotic value of the eigenstrain

$$\tilde{\epsilon}^* e \xrightarrow{e \rightarrow 0} \begin{bmatrix} 0 & 0 & \frac{4\sigma(1-\nu^2)}{\pi E e} & 0 & 0 & 0 \end{bmatrix}^T. \quad (35)$$

The explicit result describing the total displacement u_ρ and u_3 is eventually given as

$$u_\rho = -\frac{\sigma\rho(1+\nu)}{2E} \left\{ (1-2\nu) \left[\frac{(1+2\nu)(1-\nu)}{(1-2\nu)(1+\nu)} - \frac{2}{\pi} \arctan \frac{\sqrt{\eta}}{R} \right] - \frac{2\beta}{\pi\alpha} \frac{R\sqrt{\eta}}{R^2+\eta} \right\}, \quad (36)$$

$$u_3 = \frac{\sigma x_3(1+\nu)}{E} \left\{ (1-2\nu) \left[\frac{\nu(1+2\nu)}{(1+\nu)(1-2\nu)} + \frac{2}{\pi} \arctan \frac{\sqrt{\eta}}{R} \right] + \frac{2\beta - x_3^2 R^2 (R^2 + \eta)}{\pi\alpha} \frac{R}{\sqrt{\eta}} \right\}, \quad (37)$$

where the variable u_ρ represents the radial displacement $u_\rho^2 = u_1^2 + u_2^2$, $\rho = \sqrt{x_1^2 + x_2^2}$ being the radius. We have also introduced the total axial displacement u_3 and the following definitions:

$$\alpha = \rho^2 \eta^2 + x_3^2 (R^2 + \eta)^2,$$

$$\beta = (1-2\nu)(x_3^2 + \rho^2) \eta^2 + 4(1-\nu) \eta x_3^2 R^2 + (3-2\nu) x_3^2 R^4,$$

$$\eta = \frac{1}{2}(x_3^2 + \rho^2 - R^2) + \frac{1}{2}\sqrt{(x_3^2 + \rho^2 + R^2)^2 - 4R^2\rho^2}. \quad (38)$$

On the upper surface of the crack (if $x_3 \rightarrow 0^+$, $\rho < R$), the limiting relationships

$$\eta \rightarrow \frac{R^2}{R^2 - \rho^2} x_3^2 \quad \text{and} \quad \frac{\beta}{\alpha} \rightarrow 3 - 2\nu \quad (39)$$

are fulfilled and, therefore, the COD is characterized by

$$u_\rho = -\frac{\sigma\rho}{2E}(1+2\nu)(1-\nu),$$

$$u_3 = \frac{4\sigma}{\pi E}(1-\nu^2)\sqrt{R^2-\rho^2}. \quad (40)$$

Moreover, the stress along the direction of application of the mode I loading can be easily obtained as

$$T_{33} = \frac{E}{(1-2\nu)(1+\nu)} \left[\frac{\nu}{\rho} \frac{\partial(\rho u_\rho)}{\partial\rho} + (1-\nu) \frac{\partial u_3}{\partial x_3} \right], \quad (41)$$

and it is reported in Fig. 5. Such a relation can be specialized on the plane $x_3=0$ containing the circular crack at radial distance $\rho > R$, obtaining

$$T_{33} = \frac{2\sigma}{\pi} \left[\frac{R}{\sqrt{\rho^2 - R^2}} + \arctan \frac{\sqrt{\rho^2 - R^2}}{R} \right]. \quad (42)$$

This relation represents the analogous of the Inglis formula [see Eq. (24)] for the case of circular crack. Similarly, we can evaluate the stress intensity factor. The radial distance from the border of the crack is given by $\rho - R$, and the SIF is calculated as

$$K_I = \lim_{\rho \rightarrow R, x_3 \rightarrow 0} \sqrt{2\pi(\rho - R)} T_{33} = \frac{2\sqrt{R}}{\sqrt{\pi}} \sigma. \quad (43)$$

B. Pure uniaxial strain conditions

The external strain is again given by Eq. (29), which, by using Eqs. (11) and (C4), provides the asymptotic value of the equivalent eigenstrain

$$\tilde{\epsilon}^* e \xrightarrow{\sim} 0 \begin{bmatrix} 0 & 0 & \frac{4\sigma(1-\nu^2)}{\pi E e} & 0 & 0 & 0 \end{bmatrix}^T. \quad (44)$$

We observe that $\tilde{\epsilon}^*$ is identical for pure uniaxial stress [see Eq. (35)] and pure uniaxial strain conditions [see Eq. (44)] in the limit of very small aspect ratio. The final result is

$$u_\rho = -\frac{\sigma\rho(1+\nu)}{2E} \left[(1-2\nu) \left(1 - \frac{2}{\pi} \arctan \frac{\sqrt{\eta}}{r} \right) - \frac{2}{\pi} \frac{\beta}{\alpha} \frac{R\sqrt{\eta}}{R^2 + \eta} \right], \quad (45)$$

$$u_3 = \frac{\sigma x_3(1+\nu)}{E} \left[(1-2\nu) \left(\frac{\nu}{1-\nu} + \frac{2}{\pi} \arctan \frac{\sqrt{\eta}}{r} \right) + \frac{2}{\pi} \frac{\beta - x_3^2 R^2 (R^2 + \eta)}{\alpha} \frac{R}{\sqrt{\eta}} \right], \quad (46)$$

where α , β , and η are defined as in Eq. (38). The limits of the displacement on the upper crack surface are given by

$$u_\rho = -\frac{\sigma\rho}{2E} (1-2\nu)(1+\nu),$$

$$u_3 = \frac{4}{\pi} \frac{\sigma}{E} (1-\nu^2) \sqrt{R^2 - \rho^2}. \quad (47)$$

Finally, we point out that Eqs. (42) and (43) hold in the case of pure uniaxial strain mode I loading as well.

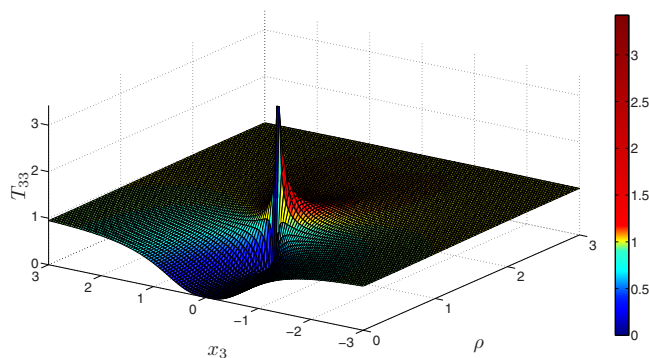


FIG. 5. (Color online) Tensile stress field T_{33} along x_3 in a circular crack. We have assumed the values $E=1$, $\sigma=1$, $\nu=0.33$, and $R=1$ in arbitrary units. The region under consideration is described by $-3 < x_3 < 3$ and $0 < \rho < 3$. The results are represented for pure uniaxial stress conditions. The color map (shown on the right) represents the intensity of T_{33} in arbitrary units.

V. DENSITY OF STATES FOR THE STRESS

The knowledge of the exact and complete solution for the elastic fields around a crack allows us to easily define and calculate the density of states for the stress field. We take into consideration the $T_{ij}(\vec{r})$ component of the stress tensor and we define its density of states $g(\tau)$ in a given region Ω ($\Omega \subset \mathfrak{R}^2$ or $\Omega \subset \mathfrak{R}^3$) as follows:

$$g(\tau) = \frac{1}{\text{mis}(\Omega)} \int_{\Omega} \delta[\tau - T_{ij}(\vec{r})] d\vec{r}, \quad (48)$$

where $\text{mis}(\Omega)$ indicates the measure of Ω (either area or volume), $\delta(x)$ is the Dirac delta function, and \vec{r} is the position vector either in two or three dimensions. If we suppose that $\tau_{\min} \leq T_{ij}(\vec{r}) \leq \tau_{\max}$ within Ω , then the following properties can be easily verified:

$$\int_{\tau_{\min}}^{\tau_{\max}} g(\tau) d\tau = 1, \quad (49)$$

$$\int_{\tau_{\min}}^{\tau_{\max}} \tau g(\tau) d\tau = \frac{1}{\text{mis}(\Omega)} \int_{\Omega} T_{ij}(\vec{r}) d\vec{r}. \quad (50)$$

Moreover, starting from Eq. (48), it can be proved that

$$g(\tau) = \frac{1}{\text{mis}(\Omega)} \int_{\{T_{ij}(\vec{r})=\tau\} \cap \Omega} \frac{1}{|\vec{\nabla} T_{ij}(\vec{r})|} ds, \quad (51)$$

which naturally underpins the possibly singular behavior of $g(\tau)$. When $\Omega \subset \mathcal{R}^2$, the set $\{T_{ij}(\vec{r}) = \tau\}$ represents a two-dimensional contour line of the component T_{ij} and, therefore, the right-hand side of Eq. (51) is a line integral (ds is the length element on the line). On the other hand, if $\Omega \subset \mathcal{R}^3$, the set $\{T_{ij}(\vec{r}) = \tau\}$ represents a three-dimensional contour surface for the component T_{ij} and the indicated operation is a surface integral (ds assumes the role of area element on such a surface).

The clear implication of Eq. (51) is that if $T_{ij}(\vec{r})$ is stationary at a given point, the integrand in the DOS expression diverges. In other words, Van Hove singularities occur in the DOS function wherever $\vec{\nabla}T_{ij}(\vec{r})=0$.²¹ A detailed analysis³⁶ shows that there are various types of Van Hove singularities in three-dimensional space, depending on whether the function goes through a local maximum, a local minimum, or a saddle point. In three dimensions, the DOS itself is not divergent, although its derivative is so and the function $g(\tau)$ shows square-root singularities. In two dimensions, the DOS is logarithmically singular, while in one dimension, the DOS itself is infinite.

Both the definition and the singular behavior of the stress DOS make this notion very similar to the one widely used in solid state physics,³⁷ for instance, to describe the distribution of electron energy states or to define the density of vibrational modes in the case of crystalline systems. Both in the electronic and phonon cases, the DOS may exhibit some singularities (Van Hove singularities).²¹ Nevertheless, some important distinctions with respect to the present elastic case should be emphasized: in the electronic case, the DOS can be measured by means of several experimental techniques and its Van Hove singularities are accessible through suitable excitations at the corresponding energies. In the mechanical counterpart, such experimental evidences are not available since, of course, a method to stimulate a given elastic response is not physically achievable. The concept of DOS in mechanical problems is nevertheless interesting and useful. Our results show that the probability density function associated with the stress field in a region containing a defect exhibits a double-peak or a triple-peak character. Therefore, the variance (or second moment) of the field is inadequate in characterizing the field fluctuations nearby the defect. To prove the importance of the local field distribution, we underline that all the moments of the stress density have a physical meaning and a practical application: in heterogeneous or composite systems, the effective physical parameters, describing the behavior at the macroscale, can be numerically obtained by means of simple averaging of the fields (i.e., stress and strain fields) over the region under consideration. So, we easily observe that the effective properties are determined from lower moments of the local fields. On the other hand, the local field distribution is also fundamental in understanding material failure or breakdown phenomena. These effects (both in dielectric and elastic context) occur at localities where the intensity of the relevant field (i.e., stress in our case) is maximum or at spots where the energy concentration is very large. Therefore, the identification of such regions and the quantification of the failure processes are based on the determination of higher order mo-

ments of the DOS. Accordingly, the stress DOS, containing the complete information on the spatial fluctuation of that field (i.e., all the possible expectation values or moments of arbitrary order), allows the quantitative evaluation of effective properties (linked to low order moments) and failure and breakdown features (linked to higher order moments).

In the following, we take into account a single crack in a solid medium and we numerically evaluate the density of state for the stress field in a given region containing the crack.

A. Slit-crack density of states

Let us consider a slit crack under tensile loading in mode I, as shown in Fig. 1. The T_{22} component of the resulting stress field can be calculated by means of Eq. (23), as reported in Fig. 4.

Two different shapes of the region Ω have been taken into consideration in order to better understand the meaning of the stress DOS. The first one is described by $-3 < x_1 < 3$ and $0 < x_2 < 3$ (corresponding to a rectangular region), and the second one by $x_1^2 + x_2^2 < 9$ and $0 < x_2 < 3$ (corresponding to a half circular region). Because of the very complicated stress field distribution, it is hard to evaluate analytically the integral appearing in Eq. (48) or in Eq. (51) and, therefore, we solved these equations numerically. The resulting DOSs for the stress field T_{22} are shown in Fig. 6. The curves of the DOS are identical both for the pure uniaxial strain and the pure uniaxial stress cases. One can observe that within the rectangular region, the DOS shows three peaks (falling at $\tau = 0.960$, $\tau = 1.009$, and $\tau = 1.019$), while within the half circular region, only two peaks are indeed found (at $\tau = 0.960$ and $\tau = 1.024$). Figure 7 reports the contour lines of the stress field for each peak of its DOS. We remark that the value assumed by the DOS at a given value τ is given by an integration over the contour $T_{22} = \tau$, weighted with a quantity inversely proportional to the modulus of the gradient of T_{22} (i.e., a quantity that increases if the function is flat). Therefore, the central lobe in Fig. 7 corresponds to the common peaks at the value $\tau = 0.960$ (see Fig. 6). This contour allows for the generation of a Van Hove singularity since it is the longer contour in that very flat zone (it is tangent to the boundary), in both the rectangular and half circular regions.

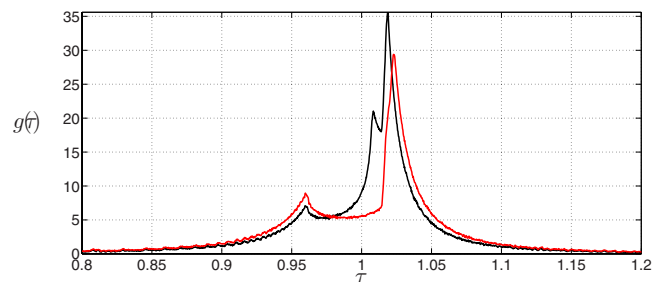


FIG. 6. (Color online) Density of states for the stress in a slit crack. The region is described by $-3 < x_1 < 3$ and $0 < x_2 < 3$ for the line with three peaks (black) and by $x_1^2 + x_2^2 < 9$ and $0 < x_2 < 3$ for the line with two peaks (red). The results are identical both for pure uniaxial stress and pure uniaxial strain conditions.

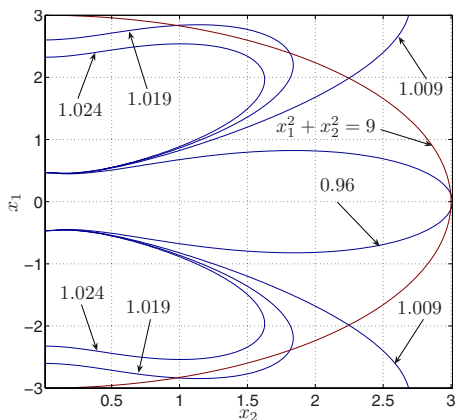


FIG. 7. (Color online) Contour lines for the function T_{22} in correspondence of the peaks exhibited by the DOS curves of Fig. 6. The lines have been computed at the values $\tau=0.960$, $\tau=1.009$, $\tau=1.019$, and $\tau=1.024$. The boundary $x_1^2+x_2^2=9$ has also been represented (red).

Moreover, the two interrupted lines in Fig. 7 correspond to the contour line at the value $\tau=1.009$. This contour has an extremal character only for the rectangular region and, therefore, a Van Hove singularity is exhibited only for such a case. Finally, the last peaks (the second in the half circular region and the third in the rectangular region, see Fig. 6) are located in very near points. The related contour lines in Fig. 7 are those with a double lobe. They have a different behavior: while the first line intersects the arc $x_1^2+x_2^2=9$ and can produce a singularity in the rectangular domain, the second line produces the singularity in the half circular domain since it does not intersect this same arc. This analysis suggests that, in order to calculate the density of states for the stress, different regions can be taken into account depending on the physical situation we are dealing with. For example, if we consider a cylindrical body with a slit crack aligned to its directrices (with the radius of the cylinder much greater than the half-length of the slit crack), we may assume a circular region (coincident with a section of the body) in order to evaluate the fluctuation distribution of the stress inside the medium. On the other hand, if we are considering a two-dimensional lattice distribution of parallel slit cracks, we

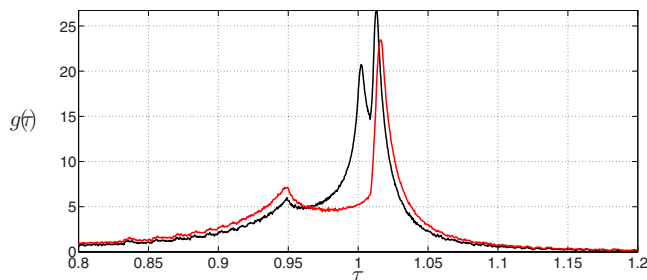


FIG. 8. (Color online) Density of states for the stress in a circular crack. The region is described by $-3 < x_3 < 3$ and $0 < \rho < 3$ for the line with three peaks (black) and by $\rho^2+x_3^2 < 9$ and $0 < \rho < 3$ for the line with two peaks (red). The results are identical both for pure uniaxial stress and pure uniaxial strain conditions.

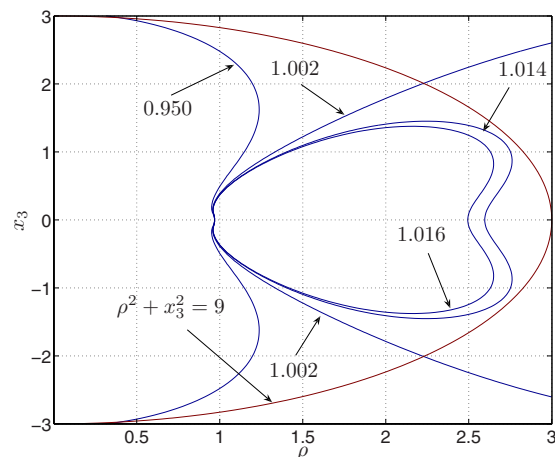


FIG. 9. (Color online) Contour lines for the function T_{33} in correspondence of the peaks exhibited by the DOS curves of Fig. 8. The lines have been computed at the values $\tau=0.950$, $\tau=1.002$, $\tau=1.014$, and $\tau=1.016$. The boundary $\rho^2+x_3^2=9$ has also been represented (red).

may consider a rectangular region (the primitive cell of the periodic structure) to evaluate the spectrum of the stress field over the entire plane.

B. Circular crack density of states

We have considered a circular crack with radius $R=1$ exposed to a tensile stress $\sigma=1$. In the case of pure uniaxial stress conditions, the results for the stress T_{33} have been shown in Fig. 5. Please note that we have assumed the values $E=1$ and $\nu=0.33$ for the elastic moduli of the matrix.

Once again, two different shapes of the region Ω have been taken into consideration in order to better understand the physical meaning of the stress DOS. The first one is described by $-3 < x_3 < 3$, and $0 < \rho < 3$, and the second one by $\rho^2+x_3^2 < 9$ and $0 < \rho < 3$. The DOS profile is identical both for the pure uniaxial strain and the pure uniaxial stress cases. The resulting DOSs for the stress field T_{33} are shown in Fig. 8. One can observe that the DOS profile shows three (two) peaks in the cylindrical region $-3 < x_3 < 3$ and $0 < \rho < 3$ (spherical region $\rho^2+x_3^2 < 9$ and $0 < \rho < 3$). The three peaks of the first DOS appear at the values $\tau=0.950$, $\tau=1.002$, and $\tau=1.014$, while the two peaks of the second DOS fall at the values $\tau=0.950$ and $\tau=1.016$. Again, this scenario can be investigated by means of the stress contour lines shown in Fig. 9. The conclusions of the previous section can be applied also in the present case.

VI. CONCLUSIONS

In the first part of this work, we have outlined a general methodology (mainly based on the external point Eshelby theory) addressed to obtaining the exact analytical expressions for the displacement field around a crack under load. The foremost achievements for mode I loading are obtained for both a slit and a circular crack. In any case, we have considered pure uniaxial stress as well as pure uniaxial strain

loading conditions. Our results are not only consistent with standard findings of LEFM, but they also generalize previous approaches and frame them into a unique picture describing the elastic behavior of a medium containing any kind of crack (or, more generally, elastic inhomogeneity). We remark that the present approach is robust enough to be applied to the more general case of an elliptic planar crack. Although this problem is not explicitly treated in the present work, such an extension could be an interesting future development since the complete analytical solution of this case is still an open problem of linear elastic fracture mechanics.

For any loading condition, the present theory allows for the exact calculation of any component of any elastic field, everywhere in the elastic solid. Therefore, within our method, the density of state for the components of the stress tensors naturally defined and calculated. This is a concept allowing a quantitative investigation on the spatial fluctuations of any mechanical quantities within a given material body. In particular, it is interesting to observe that the density of states for the tensile part of the stress around a crack exhibits some singularities. Although in this work we focused on the stress DOS for a single crack (slit or circular) embedded into a homogeneous medium, it is nevertheless possible to extend such a concept to the case of a distribution of defects or inhomogeneities. In this case, the stress DOS is valuable in characterizing the state of order of the defected solid body. Indeed, when the defects are periodically distributed in the matrix (in a crystal-like fashion), the singularities are very prominent and evident. On the other hand, when the defects are randomly distributed and oriented, the stress DOS function does not exhibit any singularity because the characteristic fluctuations of the elastic fields are smeared out by the complicated and irregular interactions among the defects.

The distribution of the local fields is of fundamental and practical importance in understanding many crucial material properties, such as breakdown phenomenon and the nonlinear behavior of composites. It is noteworthy that the DOS analysis of field fluctuations provided in this paper for mechanical quantities describing cracking processes can be, in fact, applied to other phenomena, including electromagnetic fields in heterogeneous media and velocity fields for flow through porous media.

ACKNOWLEDGMENTS

We acknowledge financial support by MIUR under project PON ‘‘CyberSar.’’ One of us (L.C.) also acknowledges support by INdAM ‘‘F. Severi’’ through the research project ‘‘Mathematical challenges in nanomechanics.’’

APPENDIX A: ELASTIC POTENTIALS FOR THE SLIT CRACK

In order to define the exact displacement field around the void inclusion, we begin by calculating the quantities $\Phi_{,i}$ and $\Psi_{,ijk}$ which appear in Eq. (5). From Eq. (6), we obtain

$$\Phi_{,i}(\vec{r}) = -\pi a_1 a_2 a_3 \int_{\eta(\vec{r})}^{+\infty} \frac{2x_i}{a_i^2 + s} \frac{ds}{R(s)} \quad (\text{A1})$$

and

$$\begin{aligned} \Psi_{,ijk}(\vec{r}) = & -\delta_{ij} \int_{\eta(\vec{r})}^{+\infty} \frac{2\pi a_1 a_2 a_3 x_k}{(a_k^2 + s)(a_j^2 + s)} \frac{sds}{R(s)} \\ & -\delta_{ki} \int_{\eta(\vec{r})}^{+\infty} \frac{2\pi a_1 a_2 a_3 x_j}{(a_j^2 + s)(a_i^2 + s)} \frac{sds}{R(s)} \\ & -\delta_{jk} \int_{\eta(\vec{r})}^{+\infty} \frac{2\pi a_1 a_2 a_3 x_i}{(a_i^2 + s)(a_k^2 + s)} \frac{sds}{R(s)} \\ & + \frac{4\pi a_1 a_2 a_3 \eta x_i x_j x_k}{(a_i^2 + \eta)(a_j^2 + \eta)(a_k^2 + \eta)R(\eta)} \frac{1}{\sum_p \frac{x_p^2}{(a_p^2 + \eta)}}. \end{aligned} \quad (\text{A2})$$

Equations (A1) and (A2) can be specialized for the present geometry ($a_1=L$, $a_2=ea_1$, $a_3 \rightarrow \infty$) getting the following set of expressions:

$$\begin{aligned} \Phi_{,1}(\vec{r}) &= -4 \frac{\pi e x_1 [L^2 + \eta - \sqrt{(L^2 + \eta)(e^2 L^2 + \eta)}]}{(1 - e^2)(L^2 + \eta)}, \\ \Phi_{,2}(\vec{r}) &= 4 \frac{\pi e x_2 [e^2 L^2 + \eta - \sqrt{(L^2 + \eta)(e^2 L^2 + \eta)}]}{(1 - e^2)(e^2 L^2 + \eta)}, \\ \Phi_{,3}(\vec{r}) &= 0, \end{aligned} \quad (\text{A3})$$

$$\Psi_{,111} = 4 \frac{\pi e x_1 \left[(3e^2 - 1) + (\eta - 3e^2 \eta - 2e^2 L^2) \sqrt{\frac{e^2 L^2 + \eta}{(L^2 + \eta)^3}} \right]}{(1 - e^2)^2} + \frac{4\pi L^2 e x_1^3 \eta \sqrt{\left(\frac{e^2 L^2 + \eta}{L^2 + \eta}\right)^3}}{2x_1^2 e^2 L^2 \eta + 2x_2^2 L^2 \eta + x_2^2 \eta^2 + x_1^2 L^4 e^4 + x_1^2 \eta^2 + x_2^2 L^4},$$

$$\Psi_{,112} = -4 \frac{\pi e x_2 \left[(1 + e^2) - (\eta + e^2 \eta + 2e^2 L^2) \sqrt{\frac{1}{(L^2 + \eta)(e^2 L^2 + \eta)}} \right]}{(1 - e^2)^2} + \frac{4\pi L^2 e x_1^2 x_2 \eta \sqrt{\frac{e^2 L^2 + \eta}{L^2 + \eta}}}{2x_1^2 e^2 L^2 \eta + 2x_2^2 L^2 \eta + x_2^2 \eta^2 + x_1^2 L^4 e^4 + x_1^2 \eta^2 + x_2^2 L^4},$$

$$\Psi_{,222} = -4 \frac{\pi e x_2 \left[(e^2 - 3) + (2e^2 L^2 - e^2 \eta + 3\eta) \sqrt{\frac{L^2 + \eta}{(e^2 L^2 + \eta)^3}} \right]}{(1 - e^2)^2} + \frac{4\pi L^2 e x_2^3 \eta \sqrt{\left(\frac{L^2 + \eta}{e^2 L^2 + \eta}\right)^3}}{2x_1^2 e^2 L^2 \eta + 2x_2^2 L^2 \eta + x_2^2 \eta^2 + x_1^2 L^4 e^4 + x_1^2 \eta^2 + x_2^2 L^4},$$

$$\Psi_{,122} = -4 \frac{\pi e x_1 \left[(e^2 + 1) - (\eta + e^2 \eta + 2e^2 L^2) \sqrt{\frac{1}{(L^2 + \eta)(e^2 L^2 + \eta)}} \right]}{(1 - e^2)^2} + \frac{4\pi L^2 e x_1 x_2^2 \eta \sqrt{\frac{L^2 + \eta}{e^2 L^2 + \eta}}}{2x_1^2 e^2 L^2 \eta + x_1^2 e^4 L^4 + x_1^2 \eta^2 + x_2^2 L^4 + x_2^2 \eta^2 + 2x_2^2 L^2 \eta},$$

$$\Psi_{,121} = \Psi_{,211} = \Psi_{,112},$$

$$\Psi_{,212} = \Psi_{,221} = \Psi_{,122}. \quad (\text{A4})$$

The elements $\Psi_{,ijk}$ not listed above are all zero. Moreover, considering the largest positive root of the corresponding quadratic algebraic equation, the quantity $\eta(\vec{r})$ defined in Eq. (7) assumes the following closed form:

$$\eta = \frac{1}{2}(x_1^2 + x_2^2 - L^2 - e^2 L^2) + \frac{1}{2} \sqrt{(x_1^2 + x_2^2 + L^2)^2 - 4L^2 x_1^2 + 2e^2 L^2 (x_1^2 - x_2^2) + e^2 L^4 (e^2 - 2)}. \quad (\text{A5})$$

It is easy to prove that the expressions given by Eqs. (A3) and (A4) approach zero when the aspect ratio e becomes vanishingly small. This is an important result since the final results (describing the actual displacement around the crack) will be obtained as a limiting process for $e \rightarrow 0$ of the product of two terms, one converging to zero and the other diverging to infinity, leading to finite outcomes.

APPENDIX B: ESHELBY TENSOR FOR ELLIPTIC CYLINDERS

The Eshelby tensor $\tilde{\mathcal{S}}$, for elliptic cylinders, is given by³

$$\tilde{\mathcal{S}} = \begin{bmatrix} M & 0 \\ 0 & N \end{bmatrix}, \quad (\text{B1})$$

where the submatrices M and N are

$$M = \frac{1}{1 - \nu} \begin{bmatrix} \frac{e}{2} \left[\frac{e+2}{(1+e)^2} + \frac{1-2\nu}{1+e} \right] & \frac{e}{2} \left[\frac{e}{(1+e)^2} - \frac{1-2\nu}{1+e} \right] & \frac{e\nu}{1+e} \\ \frac{1}{2} \left[\frac{1}{(1+e)^2} - \frac{1-2\nu}{1+e} \right] & \frac{1}{2} \left[\frac{1+2e}{(1+e)^2} + \frac{1-2\nu}{1+e} \right] & \frac{\nu}{1+e} \\ 0 & 0 & 0 \end{bmatrix},$$

$$N = \begin{bmatrix} \frac{1}{2(1-\nu)} \left[\frac{1+e^2}{(1+e)^2} + 1 - 2\nu \right] & 0 & 0 \\ 0 & \frac{1}{1+e} & 0 \\ 0 & 0 & \frac{e}{1+e} \end{bmatrix}. \quad (\text{B2})$$

It is important to notice that the tensor $\tilde{I} - \tilde{\mathcal{S}}$ appearing in Eq. (11) is singular when $e \rightarrow 0$. This result well describes the singular behavior of the strain field in flat void inclusions and it can be proved by the direct calculation of the inverse matrix,

$$[\tilde{I} - \tilde{\mathcal{S}}]^{-1} = \begin{bmatrix} (I - M)^{-1} & 0 \\ 0 & (I - N)^{-1} \end{bmatrix}, \quad (\text{B3})$$

where I is the 3×3 identity matrix. The calculations lead to these explicit results for the submatrices

$$(I-M)^{-1} = \begin{bmatrix} \frac{(1+2e-2ve-2v)(1-\nu)}{(1-2\nu)} & \frac{(2ve+2v-1)(1-\nu)}{(1-2\nu)} & \frac{(2e-2ve+2v-1)v}{(1-2\nu)} \\ \frac{(2ve+2v-e)(1-\nu)}{e(1-2\nu)} & \frac{(e-2ve-2v+2)(1-\nu)}{e(1-2\nu)} & \frac{(2ve-2v+2-e)v}{e(1-2\nu)} \\ 0 & 0 & 1 \end{bmatrix}, \quad (\text{B4})$$

$$(I-N)^{-1} = \begin{bmatrix} \frac{(1+e)^2(1-\nu)}{e} & 0 & 0 \\ 0 & \frac{1+e}{e} & 0 \\ 0 & 0 & e+1 \end{bmatrix}. \quad (\text{B5})$$

So, it is evident from Eqs. (B4) and (B5) that the eigenstrain given by Eq. (11) is singular when $e \rightarrow 0$ (some elements diverge to infinity). In particular, we may write the asymptotic relation

$$[\tilde{I} - \tilde{S}]^{-1} e \xrightarrow{\sim} 0 \begin{bmatrix} 0 & 0 & 0 & 0 & 0 & 0 \\ \frac{2\nu(1-\nu)}{(1-2\nu)e} & \frac{2(1-\nu)^2}{(1-2\nu)e} & \frac{2\nu(1-\nu)}{(1-2\nu)e} & 0 & 0 & 0 \\ 0 & 0 & 0 & 0 & 0 & 0 \\ 0 & 0 & 0 & \frac{1-\nu}{e} & 0 & 0 \\ 0 & 0 & 0 & 0 & \frac{1}{e} & 0 \\ 0 & 0 & 0 & 0 & 0 & 0 \end{bmatrix}. \quad (\text{B6})$$

Equation (B6) contains all the physical information needed to describe the behavior of a slit crack.

APPENDIX C: ESHELBY TENSOR FOR ELLIPSOIDS OF REVOLUTION

The general structure of the Eshelby tensor for the ellipsoids of revolution is given by³

$$\tilde{S} = \begin{bmatrix} \mathcal{S}_{1111} & \mathcal{S}_{1122} & \mathcal{S}_{1133} & 0 & 0 & 0 \\ \mathcal{S}_{1122} & \mathcal{S}_{1111} & \mathcal{S}_{1133} & 0 & 0 & 0 \\ \mathcal{S}_{3311} & \mathcal{S}_{3311} & \mathcal{S}_{3333} & 0 & 0 & 0 \\ 0 & 0 & 0 & \mathcal{S}_{1111} - \mathcal{S}_{1122} & 0 & 0 \\ 0 & 0 & 0 & 0 & 2\mathcal{S}_{1313} & 0 \\ 0 & 0 & 0 & 0 & 0 & 2\mathcal{S}_{1313} \end{bmatrix}. \quad (\text{C1})$$

The form of \tilde{S} correctly describes the symmetries of an ellipsoid of revolution, which has two equivalent axes and a third one with different behaviors. The complete expressions for the entries of the tensor are

$$\mathcal{S}_{1111} = \frac{1}{8} \frac{13\mathcal{L} - 3e^2 - 4e^2\mathcal{L} + 8\mathcal{L}ve^2 - 8\mathcal{L}\nu}{(1-e^2)(1-\nu)},$$

$$\mathcal{S}_{1122} = -\frac{1}{8} \frac{e^2 + \mathcal{L} - 4e^2\mathcal{L} + 8\mathcal{L}ve^2 - 8\mathcal{L}\nu}{(1-e^2)(1-\nu)},$$

$$\mathcal{S}_{1133} = -\frac{1}{2} \frac{2e^2\mathcal{L} - e^2 + \mathcal{L} + 2\mathcal{L}ve^2 - 2\mathcal{L}\nu}{(1-e^2)(1-\nu)},$$

$$\mathcal{S}_{3311} = \frac{1}{2} \frac{e^2 - \mathcal{L} - 2e^2\mathcal{L} - 2ve^2 + 2\nu + 4\mathcal{L}ve^2 - 4\mathcal{L}\nu}{(1-e^2)(1-\nu)},$$

$$\mathcal{S}_{3333} = \frac{1 - 2e^2 + 4e^2\mathcal{L} - \mathcal{L} + ve^2 - \nu - 2\mathcal{L}ve^2 + 2\mathcal{L}\nu}{(1-e^2)(1-\nu)},$$

$$\mathcal{S}_{1313} = -\frac{1}{4} \frac{e^2\mathcal{L} + 2\mathcal{L} - 1 + \mathcal{L}ve^2 - \mathcal{L}\nu - ve^2 + \nu}{(1-e^2)(1-\nu)}. \quad (\text{C2})$$

The depolarization factor \mathcal{L} depends on the shape of the ellipsoid and it can be computed in closed form. The ellipsoid is prolate (of ovary or elongated form) if $e > 1$ and oblate (of planetary or flattened form) if $e < 1$,

$$\mathcal{L} = \frac{e}{2} \int_0^{+\infty} \frac{d\xi}{(\xi+1)^2(\xi+e^2)^{1/2}} = \begin{cases} \frac{e}{4(\sqrt{e^2-1})^3} \left[2e\sqrt{e^2-1} + \ln \frac{e-\sqrt{e^2-1}}{e+\sqrt{e^2-1}} \right] & \text{if } e > 1 \\ \frac{e}{4(\sqrt{1-e^2})^3} \left[\pi - 2e\sqrt{1-e^2} - 2 \arctan \frac{e}{\sqrt{1-e^2}} \right] & \text{if } e < 1. \end{cases} \quad (\text{C3})$$

As described in Eq. (11), the relationship between the external strain and the eigenstrain is given by $\tilde{\epsilon}^* = [\tilde{I} - \tilde{S}]^{-1} \tilde{\epsilon}^\infty$. We take into consideration only the leading singular terms containing the $1/e$ divergence since we are focusing on the $e \ll 1$ case,

$$[\tilde{I} - \tilde{S}]^{-1} \tilde{\epsilon} \xrightarrow{e \rightarrow 0} \begin{bmatrix} 0 & 0 & 0 & 0 & 0 & 0 \\ 0 & 0 & 0 & 0 & 0 & 0 \\ \frac{4\nu(1-\nu)}{\pi(1-2\nu)e} & \frac{4\nu(1-\nu)}{\pi(1-2\nu)e} & \frac{4(1-\nu)^2}{\pi(1-2\nu)e} & 0 & 0 & 0 \\ 0 & 0 & 0 & 0 & 0 & 0 \\ 0 & 0 & 0 & 0 & \frac{4(1-\nu)}{\pi(2-\nu)e} & 0 \\ 0 & 0 & 0 & 0 & 0 & \frac{4(1-\nu)}{\pi(2-\nu)e} \end{bmatrix}. \quad (\text{C4})$$

As before, Eq. (C4) contains all the details necessary to model the behavior of a circular crack, obtained in the limit of the aspect ratio e approaching zero. Moreover, Eq. (C4) is the circular crack counterpart of the Eq. (B6), obtained for the slit-crack geometry.

*stefano.giordano@dsf.unica.it

†luciano.colombo@dsf.unica.it

¹L. K. H. Van Beek, *Progress in Dielectric* (Heywood, London, 1967), Vol. 7, p. 71.

²L. J. Walpole, *Adv. Appl. Mech.* **11**, 169 (1981).

³T. Mura, *Micromechanics of Defects in Solids* (Kluwer Academic, Dordrecht, 1987).

⁴Z. Hashin, *J. Appl. Mech.* **50**, 481 (1983).

⁵K. Z. Markov, in *Heterogeneous Media: Micromechanics Modeling Methods and Simulations*, edited by K. Z. Markov and L. Preziosi (Birkhauser, Boston, 2000).

⁶M. Avellaneda, *Commun. Pure Appl. Math.* **40**, 527 (1987).

⁷S. Giordano, *Eur. J. Mech. A/Solids* **22**, 885 (2003).

⁸R. McLaughlin, *Int. J. Eng. Sci.* **15**, 237 (1977).

⁹R. Hill, *J. Mech. Phys. Solids* **11**, 357 (1963).

¹⁰M. Kachanov and I. Sevostianov, *Int. J. Solids Struct.* **42**, 309 (2005).

¹¹B. Budiansky and R. J. O'Connell, *Int. J. Solids Struct.* **12**, 81 (1976).

¹²S. Giordano and L. Colombo, *Phys. Rev. Lett.* **98**, 055503 (2007).

¹³M. Kachanov, *Appl. Mech. Rev.* **45**, 305 (1992).

¹⁴L. Xiantao and E. Weinan, *J. Mech. Phys. Solids* **53**, 1650 (2005).

¹⁵J. D. Clayton and P. W. Chung, *J. Mech. Phys. Solids* **54**, 1604 (2006).

¹⁶A. Mattoni, L. Colombo, and F. Cleri, *Phys. Rev. Lett.* **95**, 115501 (2005).

¹⁷A. A. Griffith, *Philos. Trans. R. Soc. London, Ser. A* **221**, 163

(1920).

¹⁸H. Cheng and S. Torquato, *Phys. Rev. B* **56**, 8060 (1997).

¹⁹D. Cule and S. Torquato, *Phys. Rev. B* **58**, R11829 (1998).

²⁰S. Giordano, *Int. J. Appl. Electromagn. Mech.* **26**, 1 (2007).

²¹L. Van Hove, *Phys. Rev.* **89**, 1189 (1953).

²²K. B. Broberg, *Cracks and Fracture* (Academic, London, 1999).

²³J. D. Eshelby, *Proc. R. Soc. London, Ser. A* **241**, 376 (1957).

²⁴J. D. Eshelby, *Proc. R. Soc. London, Ser. A* **252**, 561 (1959).

²⁵C. E. Inglis, *Trans. RINA* **LV**, 219 (1913).

²⁶G. Kolosoff, Ph.D. thesis, Dorpat University (Estonia), 1909.

²⁷G. Kolosoff, *Z. Math. Phys.* **62**, 384 (1914).

²⁸P. F. Papkovitch, *Izv. Akad. Nauk SSSR, Ser. Fiz.-Met.* **10**, 1425 (1932).

²⁹N. I. Muskhelishvili, *Some Basic Problems in the Mathematical Theory of Elasticity* (Noordhoff, Groningen, 1953).

³⁰A. E. Green and W. Zerna, *Theoretical Elasticity* (Oxford University Press, Oxford, 1954).

³¹I. N. Sneddon, *Proc. R. Soc. London, Ser. A* **187**, 229 (1946).

³²V. I. Fabrikant, *Adv. Appl. Mech.* **27**, 153 (1990).

³³L. D. Landau and E. M. Lifschitz, *Theory of Elasticity*, Course of Theoretical Physics Vol 7, 3rd ed. (Butterworths Heinemann, Oxford, 1986).

³⁴G. R. Irwin, *J. Appl. Mech.* **24**, 361 (1957).

³⁵D. M. Barnett and R. J. Asaro, *J. Mech. Phys. Solids* **20**, 353 (1972).

³⁶F. Bassani and G. Pastori Parravicini, *Electronic States and Optical Transitions in Solids* (Pergamon, Oxford, 1975).

³⁷N. W. Ashcroft and N. D. Mermin, *Solid State Physics* (Saunders College, Orlando, 1976).